

A Flexible Commodity Skew Model with Maturity Effects

Orcan Ögetbil* and Bernhard Hientzsch†

Corporate Model Risk, Wells Fargo Bank

Abstract

We propose a non-parametric extension with leverage functions to the Andersen commodity curve model. We calibrate this model to market data for WTI and NG including option skew at the standard maturities. While the model can be calibrated by an analytical formula for the deterministic rate case, the stochastic rate case demands estimation of an expectation for which we employ Monte Carlo simulation. We find that the market smile is captured for the deterministic rate case; and with relatively low number of paths, for the stochastic rate case. Since there is typically at most one standard maturity with liquid volatility data for each futures contract, there is flexibility on the shape of nonstandard maturity implied volatility and how the total implied variance accumulates. We equip the model with different total implied variance accumulators to demonstrate that flexibility.

1 Introduction

For both pricing and traded risk management such as CVA for instruments based on futures of different maturities, one needs commodity curve models with various properties. In our particular setting, we are looking for a model that starts from a model in which a small number of Brownian factors drives the entire curve and captures ATM volatility and (imperfect) correlation (like the Andersen model) but extends it to a model in which a given implied volatility slice or a number of calibration European options on the standard expiry for each futures contract is repriced as well as possible for each futures contract separately from each other, regardless whether they follow some parametric form or not, as long as they are arbitrage free. We would like to select a model which we can calibrate by either an explicit formula from given volatility market data or by something that can be computed by Monte-Carlo through computation of expectations or through Monte-Carlo based regressions, rather than by approaches involving more computationally or implementationally complex and expensive methods such as particle filters, optimization through PDE/PIDE or FFT/Integral solvers, or similar methods. We also prefer models that can be easily evaluated and simulated at each needed time (as needed for exposure computations) with standard methodologies.

*orcan.ogetbil@wellsfargo.com

†bernhard.hientzsch@wellsfargo.com

Since for each futures contract, there is at most one liquidly traded option maturity¹, we want to have the freedom to accumulate the total implied variance from that maturity through time in a flexible way which would allow the model to mimick stylized facts in volatility behavior in the observational and/or risk-neutral measure. (Should there be more than one liquidly trade option maturity or should there be internally marked volatility slices at different maturities, we similarly could accumulate the total implied variance through time but now constrained by data on more slices.) We also want to allow additional stochastic variance or volatility factors or processes if desired.

Without skew modeling, the movement of commodity futures was modeled with two Brownian motions previously in [1], where the futures prices are derived from the modeled but not directly observable quantities such as spot commodity and a very long term futures contract that represents the long maturity asymptotic behavior.

More recently Andersen [2] suggested three different approaches to add skew to the model – jump diffusion models, stochastic volatility models, and regime-switch models (possibly combined); and further discussing regime-switch models, all on the level of the factors driving the curve and not associated to futures of particular maturities. Jump diffusion models lead to Partial Integral and Differential Equations (PIDE) and stochastic volatility models lead to FFT and integral equation such as in the famous Heston model. PIDE are quite involved to treat well, stochastic volatility models treated by FFT/characteristic function methods also require careful treatment. Stochastic volatility models typically cannot fit skews everywhere well enough; one typically needs local stochastic volatility models to fit skews well. Regime-switch model lead to a mixture of Black-Schole/lognormal formulas so they are easy to compute but mixtures of lognormals cannot fit all skews well enough. All of these models modify the form of the entire futures curve, so one has to fit skews across all maturities, either at the same time or one after the other. Andersen [2] does not give details about calibration or pricing with jump diffusion or stochastic volatility extensions. He does show an example fitting for his suggested regime-switch model. However, he did not have reliable option skew data from his trading desk and the fit to the option skew data he used was only approximate.

Following [1], modeling a fictitious spot commodity process has been studied at several occasions in the literature. In [3] a one-factor fictitious spot model is fit to the given volatility slices at the standard maturities. The authors need to introduce some freedom in the drift of the spot to be able to calibrate to the market data. Since it is a one-factor model, different futures will be perfectly correlated, but the volatility of the fictitious spot can be computed by an extended Dupire equation. They quickly mention extensions to several factors (in which the one-factor volatility term is redistributed to several factors), and to stochastic volatility factors in addition to the leverage function, but do not give details or results. There is no freedom to shape or redistribute total implied variance (or to model any non-front contract) and there is perfect correlation. [4] introduces a two-factor stochastic local volatility fictitious spot model (two spot processes) so that futures options and index options can be priced, modeling the front two contracts at different times, capturing the correlation between them, and calibrating the models with particles filters. While the front

¹For some delivery months, liquid option trading for the standard maturity might not have started yet and hence those contracts might not have liquid volatility data yet. In those circumstances, we use an accumulator derived from the implied volatility of the next liquidly traded longer contract.

two contracts can be modeled, no other futures contracts are modeled in detail.

[5, 6, 7] introduce stochastic volatility multi-factor models where each Brownian curve driving factor is associated with its own CIR-type stochastic volatility factor with a time-dependent seasonal mean. They introduce the model both in risk-neutral and observational measure, describe FFT based pricing (and calibration) for the risk-neutral setting, and a Kalman filter for its use under the observational measure. They explicitly introduce terms to introduce maturity ("Samuelson") effects. They demonstrate reasonable good fitting of option skews but not all option quotes can be fit (see [7, version 3: Figure 3 on page 28]). Pricing and calibration in these models require FFT and/or direct integration approaches with careful treatment of characteristic functions and domain or contour of integration and possibly need damping. We are looking for a model set-up which allows calibration and pricing with simpler methodologies.

A model in both physical \mathbb{P} and risk-neutral \mathbb{Q} measures is presented in [8] that can at most fit at-the-money (ATM) volatility and has no more degrees of freedom for the skew. However, this model could be extended to capture skew similarly how we add skew to the Andersen model in this paper. [9] models the skew in the observational measure and discusses option pricing. It involves very heavy mathematical machinery and does not fit easily in the standard simulation set-ups. It does not demonstrate calibration to option prices. Futures curves driven by time-changed Ornstein-Uhlenbeck processes are modeled in [10], including with additional stochastic volatility which can also fit common skew shapes in their examples. Modeling and calibration are quite involved and time-changed processes do not fit well into the standard simulation set-up.

Instead, in our work we add separate leverage functions as multipliers for each modeled futures, and discuss how to calibrate the resulting model by formula (for deterministic rates) or by computing MC expectations (for stochastic rates); and will review how this model satisfies all of our requirements as discussed earlier.

The structure of the paper is as follows. Section 2 reviews Andersen's two-factor model and shows how it calibrates to recent market data for WTI and NG. In Section 3, we extend this model with leverage functions. We outline steps for calibration of leverage functions for both deterministic and stochastic rate cases, and demonstrate that the calibrated model captures the market smile. We propose a method to shape the forward implied volatility (through the remaining total implied variance) of options on futures with longer deliveries according to the implied volatility of corresponding options on futures with shorter deliveries and also mention other ways to control the accumulation of total implied variance for futures options with longer deliveries. In Section 4 we briefly discuss our findings.

2 Andersen's Markov Diffusion Model on Commodity Futures

We start with reviewing the diffusion model proposed by Andersen [2]. Motivated by principal component analysis on historical futures returns and practicality reasons, futures price curve movements are governed by two Brownian motions. Let W_1 and W_2 be *independent* Brownian motions under risk-neutral measure \mathbb{Q} of filtered probability space $(\Omega, \mathcal{F}, \{\mathcal{F}_t, t \geq 0\}, \mathbb{Q})$. Let us denote the futures delivery times by $T_j, j = 1, \dots, J$. Here J

depends on data availability and is different for each commodity underlier. The price of a futures contract $F_j(t)$ with delivery time T_j evolves by

$$dF_j(t) = F_j(t) [\sigma_1(t, T_j)dW_1(t) + \sigma_2(t, T_j)dW_2(t)]. \quad (2.1)$$

Here the deterministic functions $\sigma_1(t, T)$ and $\sigma_2(t, T)$ are given by

$$\sigma_1(t, T) = e^{b(T)-\kappa(T-t)}h_1 + e^{a(T)}h_\infty, \quad \sigma_2(t, T) = e^{b(T)-\kappa(T-t)}h_2, \quad (2.2)$$

where the model parameters h_1, h_2, h_∞ are constants; $\kappa \geq 0$ is mean reversion speed; $a(T), b(T)$ are seasonality adjustment functions oscillating around zero at an annual frequency. The following parametrization allows us to write the model parameters in terms of more intuitive quantities.

$$\sigma_0 \equiv \sqrt{(h_1 + h_\infty)^2 + h_2^2}, \quad \sigma_\infty \equiv h_\infty, \quad \rho_\infty \equiv \frac{h_1 + h_\infty}{\sqrt{(h_1 + h_\infty)^2 + h_2^2}}. \quad (2.3)$$

In this parametrization, σ_0 and σ_∞ represent the short term and long term futures price volatilities in the absence of seasonality, and ρ_∞ is the correlation between the price changes of the spot and the long-end of the futures curve. The at-the-money market implied volatility is related to the model parameters as [2],

$$\Sigma^{\text{ATM}}(T)^2 = (h_1^2 + h_2^2)e^{2b(T)}\frac{1 - e^{-2\kappa T}}{2\kappa T} + 2h_\infty h_1 e^{a(T)+b(T)}\frac{1 - e^{-\kappa T}}{\kappa T} + h_\infty^2 e^{2a(T)}. \quad (2.4)$$

We calibrate the model parameters to the market data following the recipe outlined in [2]. First, we study the correlation structure. Setting $X(t, T_j) \equiv \log F_j(t)$, through the correlation function

$$\rho(t, \Delta_1, \Delta_2) = \text{corr}(dX(t, t + \Delta_1), dX(t, t + \Delta_2)) \quad (2.5)$$

we define a function to measure the time dependence of correlations

$$f_\infty(t) \equiv \lim_{\Delta \rightarrow \infty} \rho(t, 0, \Delta). \quad (2.6)$$

We analyze futures returns data for WTI and NG to estimate $f_\infty(t)$ empirically using $\rho(t, 1 \text{ month}, 48 \text{ months})$ as a proxy to this quantity. According to Figure 2.1, the correlation structure does not show a clear seasonal trend, thus we can model it as time-stationary, $f_\infty(t) = \rho_\infty$, and $a(T) = b(T)$. We estimate $\rho_\infty = 0.7$ for WTI and $\rho_\infty = 0.2$ for NG. In Figure 2.2, we see that these estimations fit the price change data reasonably well, even on those months with lower empirical correlations.

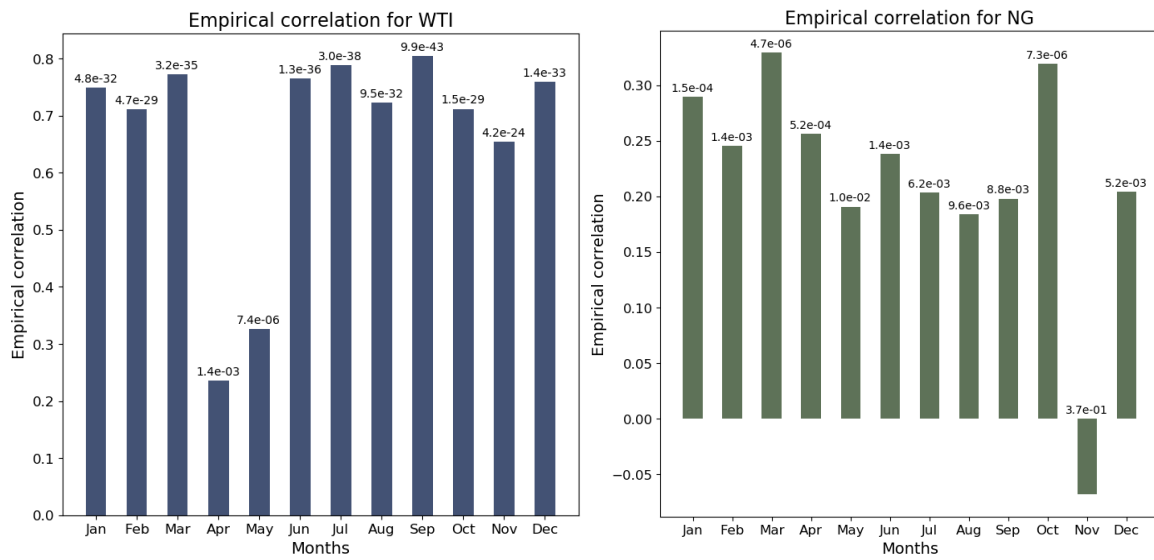


Figure 2.1: Estimating $f_{\infty}(t)$ empirically for WTI and NG data between 2013-01-01 and 2021-12-31, as a function of the calendar month of t . The number above each bar is the corresponding p-value.

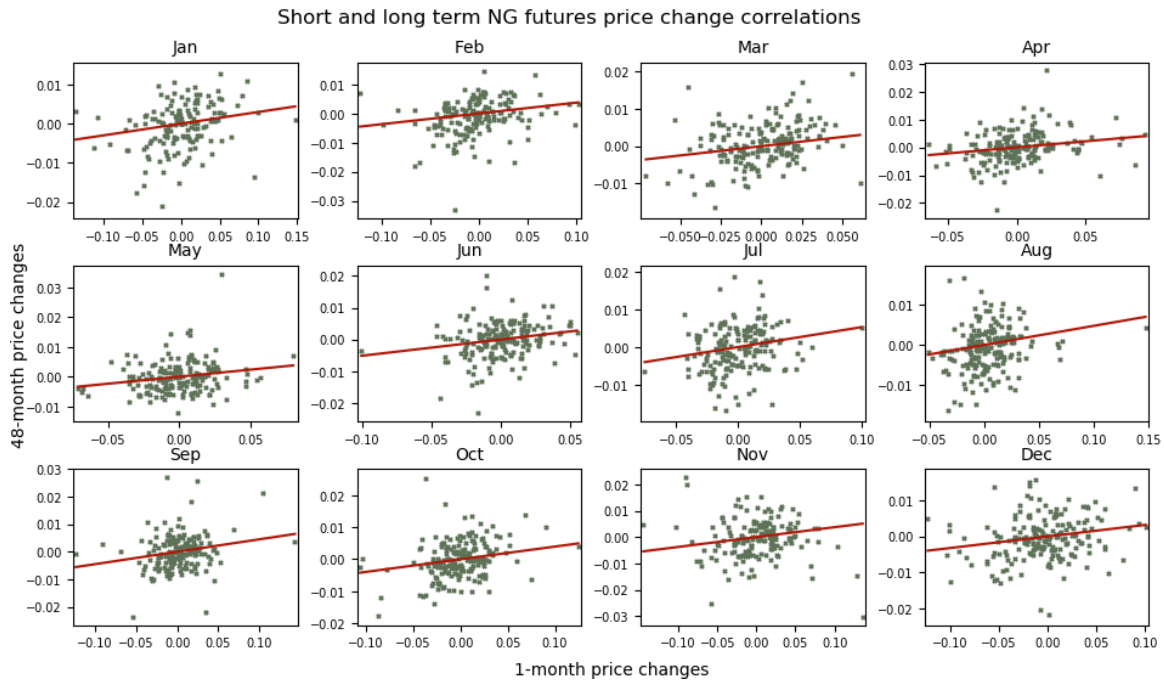
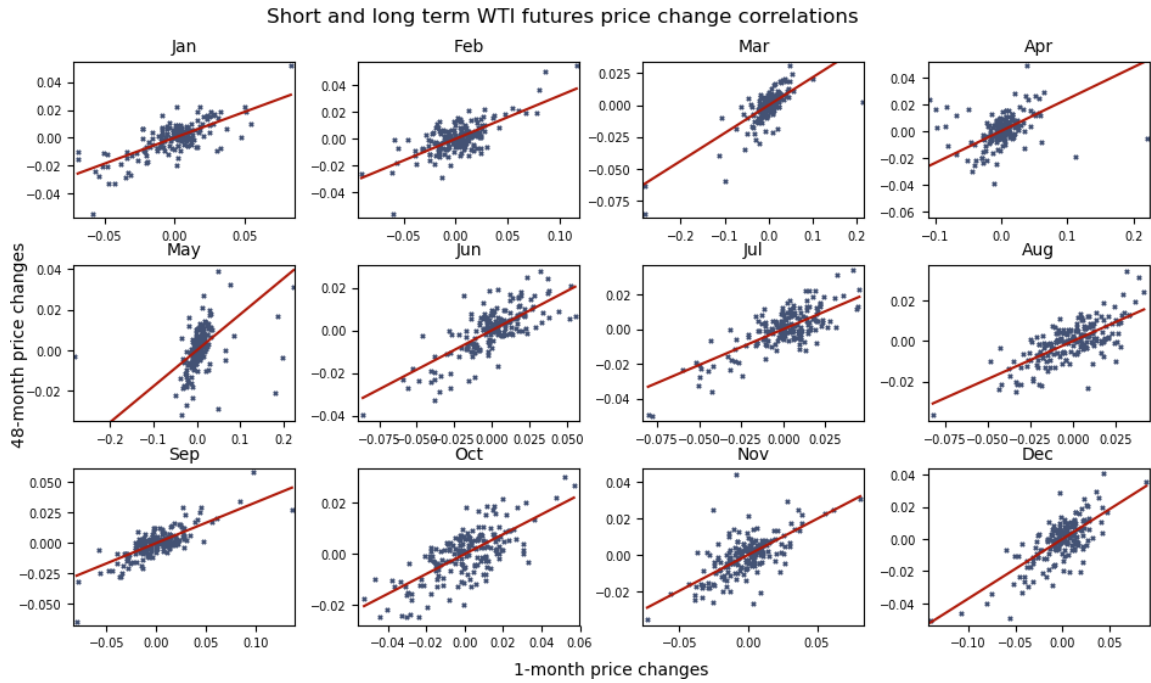


Figure 2.2: Daily price changes of 1-month and 48-month expiry futures of WTI and NG data between 2013-01-01 and 2021-12-31, for each month of the year. The red lines correspond to the estimated values $\rho_\infty = 0.7$ for WTI and $\rho_\infty = 0.2$ for NG.

The rest of the parameters are calibrated to the market implied volatility data as of 2021-12-31 by (2.4) as $\kappa = 0.2657, h_1 = 0.2365, h_2 = 0.2970, h_\infty = 0.0546$ for WTI and $\kappa = 2.3562, h_1 = -0.0634, h_2 = 0.5854, h_\infty = 0.1829$ for NG, with $a(T)$ as given in Figure 2.3.

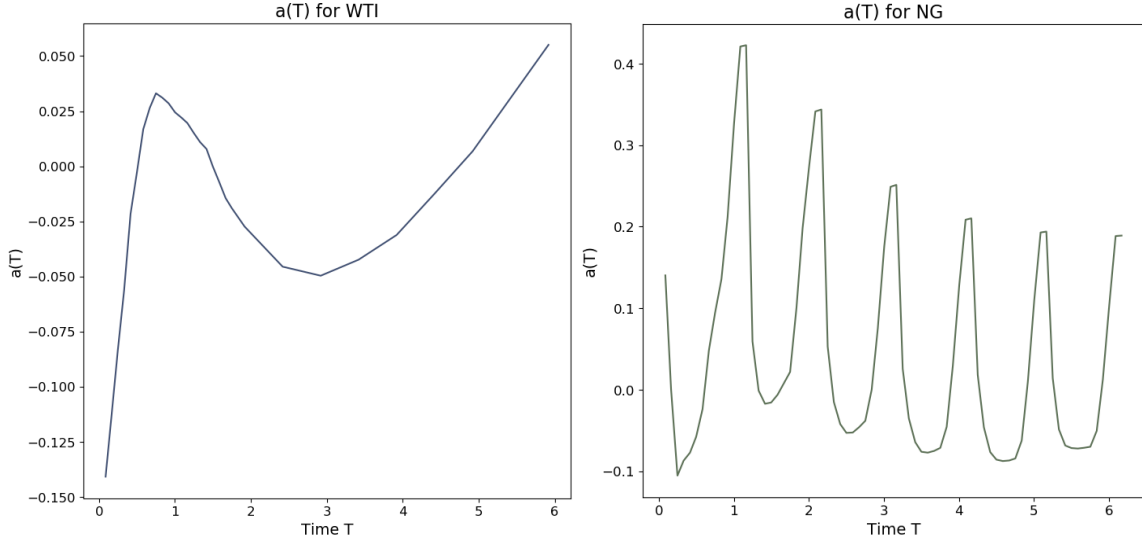


Figure 2.3: Seasonality adjustment function $a(T)$ for WTI and NG computed by Lemma 10 of [2] based on implied volatility data as of 2021-12-31.

We simulate the model with the above calibrated parameters to price vanilla call options. First we price at-the-money vanilla call options at various expiries, and by inverting the Black formula we evaluate the implied volatility from Monte Carlo prices as well as Monte Carlo prices bumped by ± 2 Monte Carlo standard errors. Figure 2.4 shows that the ATM market implied volatility is well recovered by the model with the calibrated parameters.

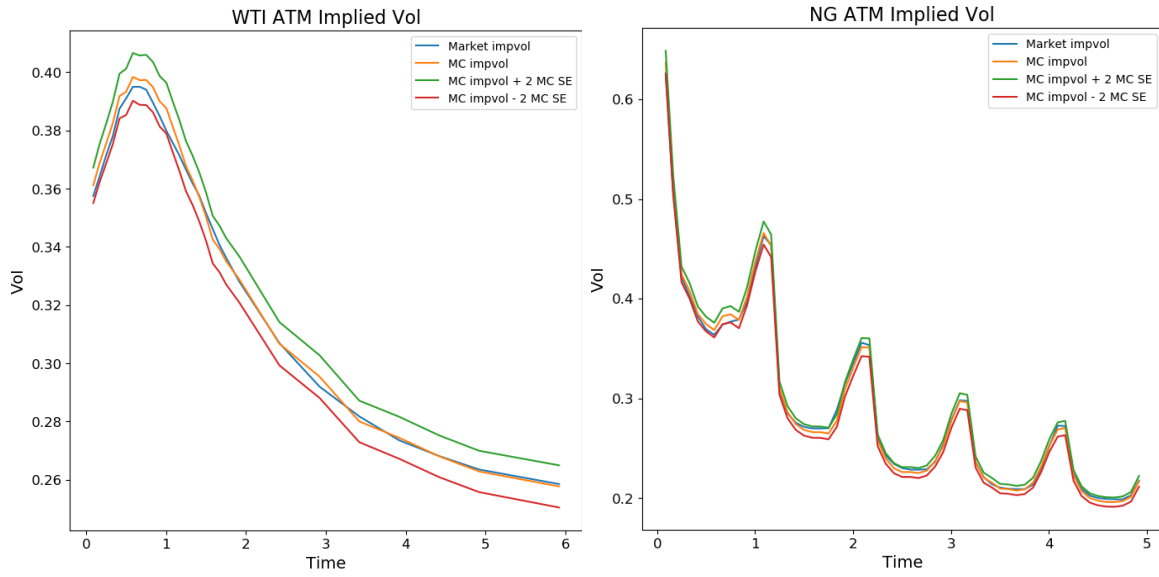


Figure 2.4: Market and Monte Carlo at-the-money (ATM) implied volatility for WTI and NG

Next we simulate the same model to price vanilla call options at various moneynesses and maturities. Here we compare Monte Carlo prices to market prices as given by market implied volatility data. Figure 2.5 shows that while the model performs well at at-the-money region (around moneyness $K/F_j(0) = 1$), the differences to market prices are significantly greater than Monte Carlo standard errors in most other regions.

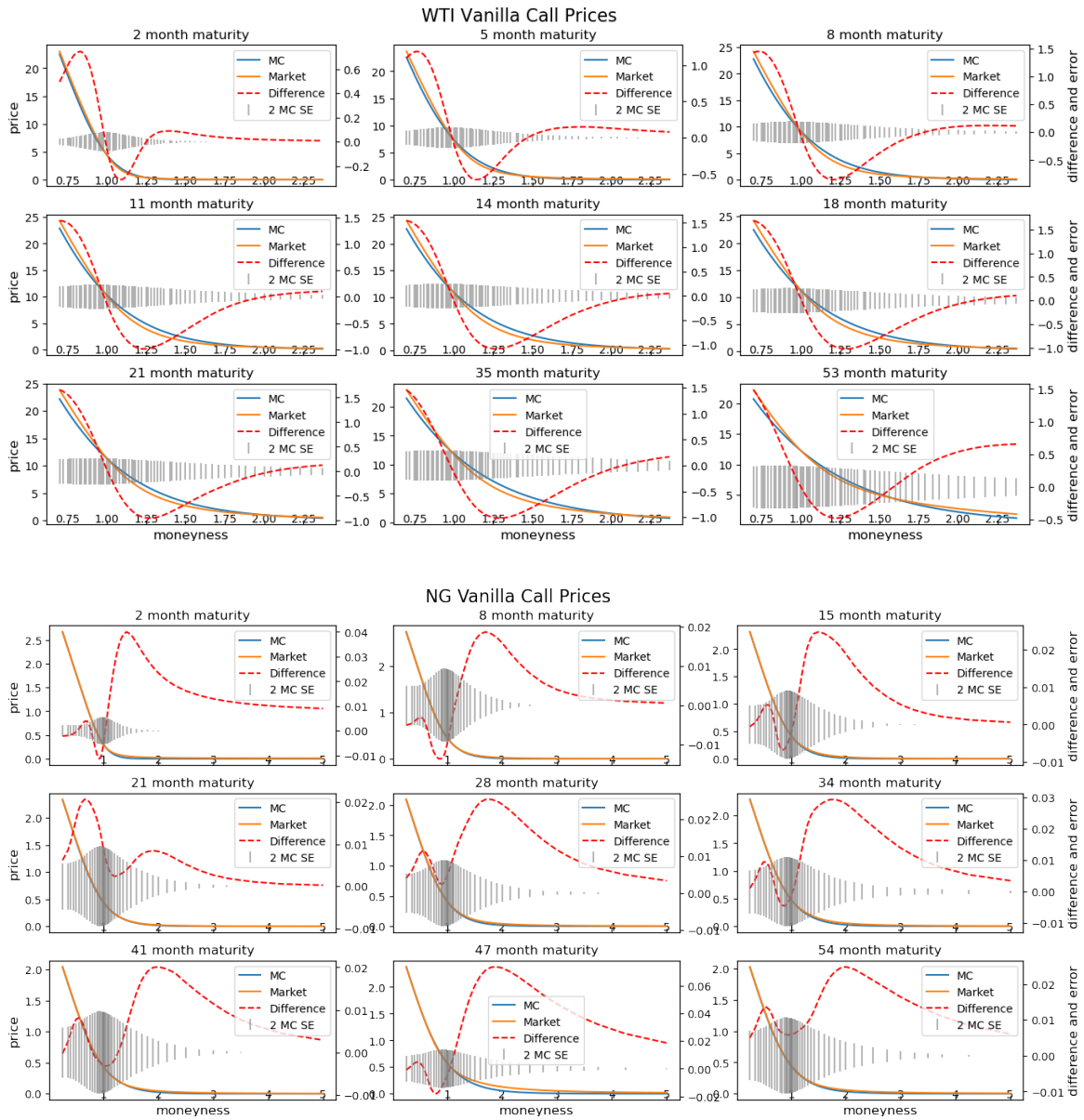


Figure 2.5: Monte Carlo prices compared to market prices for WTI and NG for various maturities and moneynesses

3 Modeling the Smile

While the above model reproduces the at-the-money implied volatilities, it performs poorly on the wings of the WTI and NG implied volatility surfaces. The original work of Andersen proposes an extension with a regime switching jump model with parameters approximately fit to capture some skew information from the market and/or desk volatility smile. Here we take a non-parametric local volatility approach.

3.1 The Leverage Functions

We generalize the model (2.1) as

$$dF_j(t) = F_j(t)L_j(F_j(t), t) [\sigma_1(t, T_j)dW_1(t) + \sigma_2(t, T_j)dW_2(t)]. \quad (3.1)$$

We formulate the model with unique leverage functions $L_j(K, t)$ for each futures delivery. For each futures delivery, there is only at most one standard liquidly quoted and traded option maturity T_j with maturity during the time when this futures contract will be the next one to be delivered.² Thus, only a single time slice T_j of implied volatility data $\Sigma_j(K, T_j)$ will be available for $F_j(t)$. The leverage functions $L_j(K, t)$ will be calibrated to this data.

We assume that the numéraire associated with the risk-neutral measure \mathbb{Q} , that is the money market account $B(t)$, accrues at short rate $r(t)$ by $dB(t) = r(t)B(t)dt$. The short rate is modeled by a single factor process of generic form

$$dr(t) = \alpha(\omega, t)dt + \sigma(\omega, t)dW^r(t), \quad (3.2)$$

where α and σ are bounded functions of a general set of stochastic factors $\omega \in \Omega$, and W^r is a Brownian motion under risk-neutral measure \mathbb{Q} . The discount factor is given by $D(t) \equiv 1/B(t) = \exp\left[-\int_0^t r(u)du\right]$.

We denote by $P(t, T) \equiv \mathbf{E}^{\mathbb{Q}}\left[\frac{D(T)}{D(t)}\middle|\mathcal{F}_t\right]$ the time t value of the zero coupon bond maturing at time T , through which we define the instantaneous forward rate

$$f(t, T) \equiv -\frac{\partial \log P(t, T)}{\partial T} = -\frac{1}{P(t, T)} \frac{\partial P(t, T)}{\partial T}. \quad (3.3)$$

Let $C_j = C_j(K, t)$ denote the time-zero price of a vanilla call option with strike K and expiry $t \leq T_j$ written on F_j . In the vanilla call option price formulation, the leverage functions for the futures with delivery T_j are given by [11]

$$L_j(K, t)^2 = \frac{\frac{\partial C_j}{\partial t} + \mathbf{E}^{\mathbb{Q}}\left[D(t)(F_j(t) - K)r(t)\mathbb{1}_{F_j(t) > K}\right]}{\frac{1}{2}K^2 \frac{\partial^2 C_j}{\partial K^2} [\sigma_1(t, T_j)^2 + \sigma_2(t, T_j)^2]}, \quad (3.4)$$

where the expectation is taken under risk-neutral measure.

3.2 Total Implied Variance Accumulation

Evaluating the call option price derivative above in time direction is not trivial as the market quotes data comes in a single time slice. The total implied variance, on the other hand, grows in time and has value zero at time zero, and hence is more straightforward to differentiate in time direction.

It is convenient to parametrize the total implied variance w_j for the vanilla options expiring at time t , written on spot futures delivered at time T_j in terms of *log-moneyness*

$$y_j(K, t) \equiv \log \frac{K}{F_j(t)}. \quad (3.5)$$

²For some delivery months, liquid option trading for the standard maturity might not have started yet and hence those contracts might not have liquid volatility data yet. In those circumstances, we use an accumulator derived from the implied volatility of the next liquidly traded longer contract.

We assume that the input implied volatility surface is transformed into log-moneyness coordinates as $\Sigma_j(y, t)$. Here we use the same log-moneynesses at all maturities and we drop the subscript j from y_j . The total implied variance is given by

$$w_j(y, t) \equiv \Sigma_j(y, t)^2 t,$$

where $\Sigma_j(y, t)$ is the implied volatility of a vanilla option expiring at time $t \leq T_j$ struck at $K = F_j e^y$, written on F_j . By means of the available implied volatility data $\Sigma_j(y, T_j)$ we compute $\tilde{w}_j(y) \equiv w_j(y, T_j)$ for all y given in the data set. We also know $w_j(y, 0) = 0$. The total implied variance is monotonically increasing between the two slices, but otherwise we have control over how quickly the total implied variance will accumulate toward its given final value.

A straightforward approach would be to model accumulation at a constant rate in time direction, creating a linear accumulator as

$$w_j(y, t) = \Sigma_j(y, T_j)^2 t = \tilde{w}_j(y) \frac{t}{T_j}, \quad 0 \leq t \leq T_j \quad (\text{linear accumulator}) \quad (3.6)$$

With a quadratic function, the total implied variance accumulates faster towards delivery,

$$w_j(y, t) = \tilde{w}_j(y) \left(\frac{t}{T_j} \right)^2, \quad 0 \leq t \leq T_j \quad (\text{quadratic accumulator}) \quad (3.7)$$

As an alternative, we can use the implied volatility from options of futures closer to their maturity which would correspond to the assumption that options with the same time-to-maturity should have the same or similar implied volatility. Thus, when the T_j futures option is T_k ($k < j$) away from its maturity (at time $T_j - T_k$), its remaining total implied variance should be the total implied variance from the T_k futures option. Thus, we propose that from time $T_j - T_k$, $k \leq j$ to time T_j a total implied variance of $\tilde{w}_k(y) \equiv \Sigma_k(y, T_k)^2 T_k$ accumulates. With this assumption, the total implied variance is $\tilde{w}_j(y) - \tilde{w}_k(y)$ at time $T_j - T_k$. Setting $T_0 \equiv \tilde{w}_0(y) \equiv 0$, we create a piecewise linear total implied variance interpolator at times $\{T_j - T_k; k = j, \dots, 0\}$ and values $\{\tilde{w}_j(y) - \tilde{w}_k(y); k = j, \dots, 0\}$ as

$$w_j(y, t) = \tilde{w}_j(y) - \tilde{w}_k(y) + \frac{\tilde{w}_k(y) - \tilde{w}_{k-1}(y)}{T_k - T_{k-1}} (t - T_j + T_k), \quad 0 \leq t \leq T_j \quad (\text{TTM IV accumulator}) \quad (3.8)$$

where $k = \operatorname{argmin}_{i \in \{1, \dots, j\}} \{T_j - T_i \leq t\}$. The procedure is repeated for every target delivery T_j so that each delivery has its own total implied variance accumulator. When implementing this mimicking approach one needs to make sure that the total implied variance remains positive and monotonically increasing. If the short term futures volatilities are sufficiently high, it is possible that the total implied variance only starts to accumulate close to the maturity for some futures. Figure 3.1 sketches the three schemes.

Instead of taking implied volatility from futures option with shorter time-to-maturity as interpolation targets, one could introduce weighting factors $W_{k,j}$ or functions, either associated with option maturity times T_k or fixed times to maturity $T_{j,k} = T_j - T_k$ with $w_j(y, T_k) = W_{k,j} w_j(y, T_j)$ or $w_j(y, T_k) = W_{k,j} w_j(y, T_{j,k})$, controlling the accumulation of the total implied variance without changing or controlling the shape and skew. While there

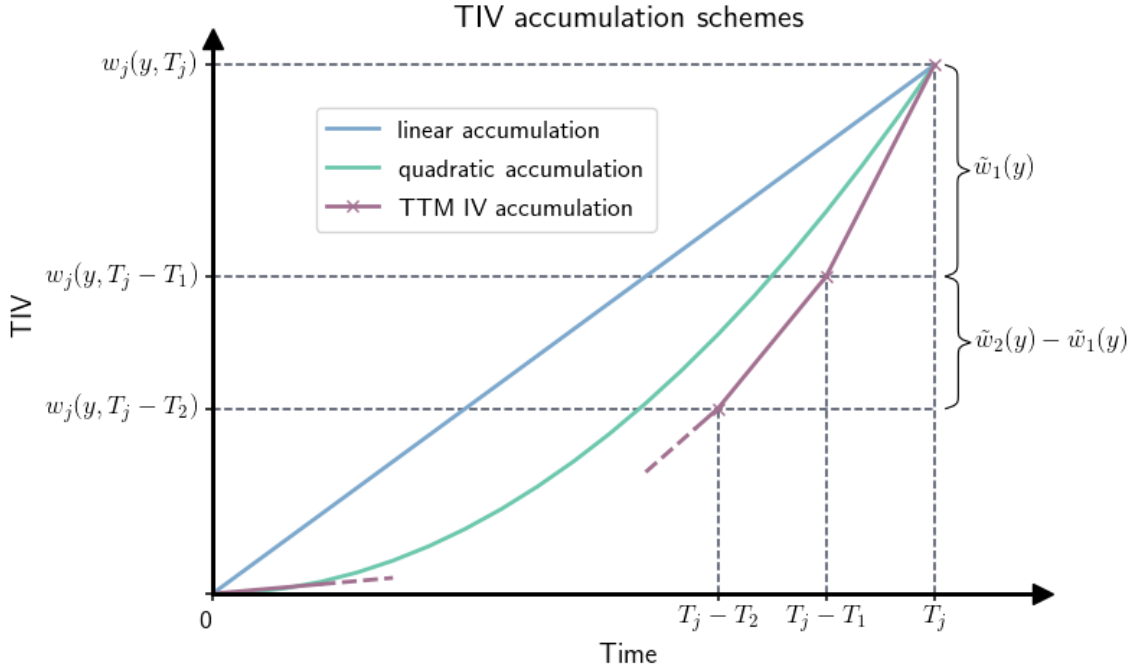


Figure 3.1: Different approaches to accumulate $w_j(y, t)$ at a given y along time dimension between times 0 and T_j , and values 0 and $\tilde{w}_j(y) = w_j(y, T_j)$. In the market mimicking accumulation scheme, one uses volatility data $\tilde{w}_k(y)$, $k < j$ from previous slices.

is some disagreement about how to measure the Samuelson maturity effect, there seems to be agreement that at least for certain commodity futures (agricultural and energy-related), there is in general larger volatility (in the sense of realized quadratic variance or volatility) or range of those futures prices (agricultural and energy) the closer the delivery of the futures (and the maturity of the option) is³. This would correspond to small and slowly increasing weighting factors when the option is far from its maturity and to larger and faster increasing weighting factors closer to its maturity. Similarly, one could replace $\frac{t}{T_j}$ in (3.6) by a function $f(\frac{t}{T_j})$ with $f(0) = 0$ and $f(1) = 1$ that expresses the maturity effect, like $f(x) = \frac{e^x - 1}{e - 1}$.

Finally, one could take a mixture of the above strategies. In this, a variety of maturity effects can be flexibly implemented while maintaining calibration to the given option skew data.

In log-moneyness parametrization, the Black-Scholes European call option price function C_j can be written as

$$C_j(P(0, t)F_j(0), y, w_j(y, t)) = P(0, t)F_j(0) (N(d_1) - e^y N(d_2)) \quad (3.9)$$

³See, for instance, [12] or [13].

with

$$\begin{aligned} d_1 &\equiv -yw_j^{-\frac{1}{2}} + \frac{1}{2}w_j^{\frac{1}{2}}, \\ d_2 &\equiv d_1 - w_j^{\frac{1}{2}}, \end{aligned}$$

and $N(\cdot)$ is the cumulative Gaussian probability distribution function. The derivatives of the call option price are computed as

$$\begin{aligned} \frac{1}{2}K^2 \frac{\partial^2 C_j}{\partial K^2} &= \frac{\partial C_j}{\partial w_j} \left[1 - \frac{y}{w_j} \frac{\partial w_j}{\partial y} + \frac{1}{2} \frac{\partial^2 w_j}{\partial y^2} + \frac{1}{4} \left(\frac{\partial w_j}{\partial y} \right)^2 \left(-\frac{1}{4} - \frac{1}{w_j} + \frac{y^2}{w_j^2} \right) \right], \\ \frac{\partial C_j}{\partial t} &= \frac{\partial C_j}{\partial w_j} \frac{\partial w_j}{\partial t} - f(0, t)C_j, \end{aligned} \quad (3.10)$$

where

$$\frac{\partial C_j}{\partial w_j} = \frac{1}{2}P(0, t)F_j(0)e^y N'(d_2)w_j^{-\frac{1}{2}}. \quad (3.11)$$

Plugging the quantities (3.10) into the identity for the leverage functions (3.4), we find

$$L_j(y, t)^2 = \frac{\frac{\partial C_j}{\partial w_j} \frac{\partial w_j}{\partial t} - f(0, t)C_j + \mathbf{E}^{\mathbb{Q}} [D(t)F_j(t)(1 - e^y)r(t)\mathbf{1}_{y < 0}]}{\frac{\partial C_j}{\partial w_j} \left[1 - \frac{y}{w_j} \frac{\partial w_j}{\partial y} + \frac{1}{2} \frac{\partial^2 w_j}{\partial y^2} + \frac{1}{4} \left(\frac{\partial w_j}{\partial y} \right)^2 \left(-\frac{1}{4} - \frac{1}{w_j} + \frac{y^2}{w_j^2} \right) \right] [\sigma_1(t, T_j)^2 + \sigma_2(t, T_j)^2]}, \quad (3.12)$$

with C_j and $\frac{\partial C_j}{\partial w_j}$ as given in (3.9) and (3.11). The above expression can be used to compute leverage functions $L_j(y, t)$ for each futures underlier $F_j(t)$ iteratively in a bootstrapping fashion.

Deterministic rate limit In this case we have $\alpha(\omega, t) = \partial f(0, t)/\partial t$, $\sigma(\omega, t) = 0$, $r(t) = f(0, t)$, and (3.4) simplifies to

$$L_j(K, t)^2 = \frac{\frac{\partial C_j}{\partial t} + f(0, t)C_j}{\frac{1}{2}K^2 \frac{\partial^2 C_j}{\partial K^2} [\sigma_1(t, T_j)^2 + \sigma_2(t, T_j)^2]}. \quad (3.13)$$

In the total implied variance formulation this can be written as

$$L_j(y, t)^2 = \frac{\frac{\partial w_j}{\partial t}}{\left[1 - \frac{y}{w_j} \frac{\partial w_j}{\partial y} + \frac{1}{2} \frac{\partial^2 w_j}{\partial y^2} + \frac{1}{4} \left(\frac{\partial w_j}{\partial y} \right)^2 \left(-\frac{1}{4} - \frac{1}{w_j} + \frac{y^2}{w_j^2} \right) \right] [\sigma_1(t, T_j)^2 + \sigma_2(t, T_j)^2]}. \quad (3.14)$$

3.3 Calibrating the Leverage Functions

We adapt the calibration approach proposed in [14] to compute the leverage functions $L_j(\cdot, t)$ for every futures delivery $F_j(t)$ simultaneously time slice by time slice. In the deterministic rate case, the calibration is straightforward since all quantities in (3.14) are known. For stochastic rate, we perform a Monte Carlo simulation to estimate the expectation appearing in (3.12).

Inputs for calibration Our calibration routine expects the following quantities as input for leverage function calibration:

- Andersen model (2.1) parameters calibrated to market data
- Futures prices $F_j(0)$ as of the valuation time $t = 0$
- Market implied volatility $\Sigma_j(y, T_j)$ for each maturity
- Market yield curve $P(0, T)$
- For a stochastic rate model, a short rate model with parameters calibrated to market data.
- For a stochastic rate model, coefficients of correlation between the short rate and the two Brownian motions of the Andersen model

Steps for calibration We calibrate the leverage functions time slice by time slice, in a bootstrapping fashion. Let $t_i; i = 1, \dots, n$ be the increasing sequence of (positive) times where we will perform the calibration.

1. Using the market implied volatilities $\Sigma_j(y, T_j)$, generate a total implied variance surface $w_j(y, t)$ interpolator. The interpolator must be able to compute the partial derivatives appearing in the local volatility expressions.
2. For the first time slice t_1 , evaluate the deterministic equation (3.14) to compute the leverage function values $L_j(y, t_1)$ for a predetermined range of strikes for every j . This step requires no Monte Carlo simulation. As a result, obtain leverage function values to be used until time t_2 in the subsequent calibration steps.
3. For each of the subsequent time slices $t_i, i > 1$, (a) deterministic rate case: evaluate (3.14) directly for a predetermined range of strikes for every j , (b) stochastic rate case: Simulate the SDE system (3.1), (3.2) up to time t_i . Compute the Monte Carlo estimate for the expectation appearing in (3.12) for a predetermined range of strikes for every j . Use these equations to obtain the leverage function values $L_j(y, t_i)$. These values will be used during subsequent simulation steps from time t_i to time t_{i+1} . This step is first performed with $i = 2$ and is then repeated for the remaining time slices.

The leverage functions strike grid is chosen uniformly in a region covered by the implied volatility data.

3.4 Implementation Tests

We apply the above recipe to market data for WTI and NG as of 2021-12-31 and compute the leverage functions $L_j(y, t)$. In Figure 3.2, we observe the leverage functions under linear (3.6), quadratic (3.7), and TTM IV (3.8) accumulation schemes described in the previous subsection, for the WTI futures underlier with 12-month delivery. As expected, the leverage function is smooth in the linear case whereas most of the magnitude and variation of the leverage function occurs closer to maturity in the nonlinear cases.

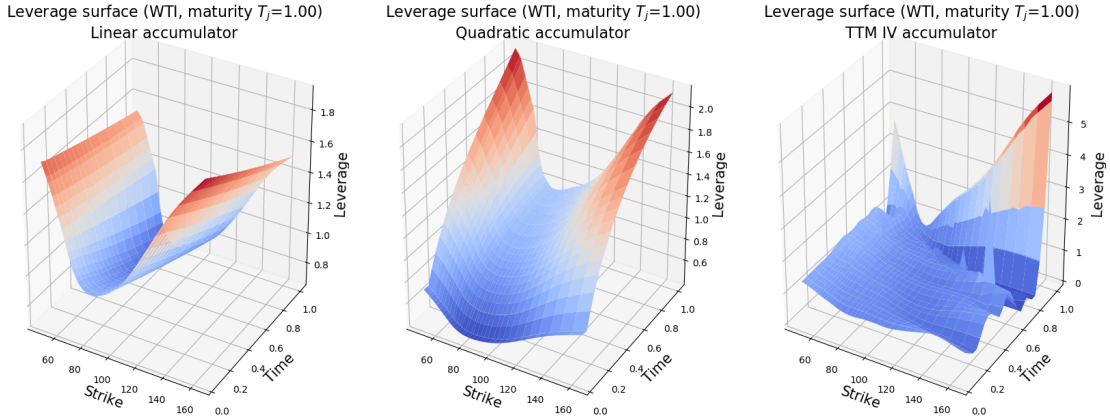


Figure 3.2: Leverage functions, computed with linear accumulation between times 0 and T_j (left), computed with quadratic accumulation (center), computed with nonlinear accumulation based on total implied variances from option prices with shorter time-to-maturity (right).

To investigate the variance accumulation of the underlying futures, we simulate the calibrated model on a time partition $\{t_s^{(j)}; s = 0, \dots, m_s\}$ with $t_0^{(j)} = 0; t_{s-1}^{(j)} < t_s^{(j)}$; and $t_{m_s}^{(j)} = T_j$ for several deliveries T_j over 10000 paths. We compute the Monte Carlo estimate and error of the realized variance $RV_j(t) \equiv \sum_{s=0}^{t_s=t} \left[\log \frac{F_j(t_s)}{F_j(t_{s-1})} \right]^2$ for the simulated model. In Figure 3.3 we plot the realized variance as a function of delivery month for several t s. One observes that the realized variance increases with t . Moreover the realized variance is higher when t is near the delivery T_j , also steeper for nonlinear accumulators near the delivery; and it decreases in general as the delivery is further from t . Figure 3.4 shows the realized

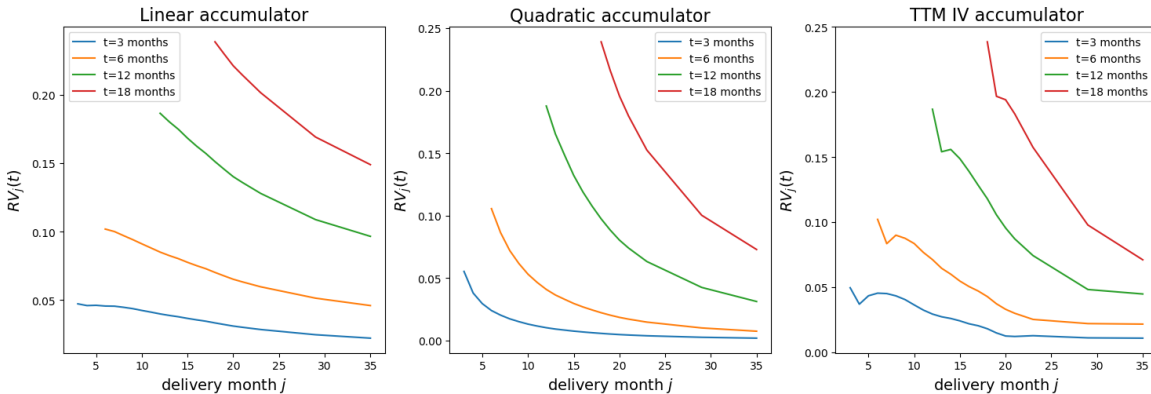


Figure 3.3: Realized variance $RV_j(t)$ for several t as a function of delivery month j estimated by Monte Carlo simulation with 10000 paths, using linear, quadratic, and TTM IV accumulators.

variance for the three total implied variance accumulation approaches we considered. As we expected, the methodologies result in the same realized variance at the delivery up to

Monte Carlo estimation errors. We also see that the total implied variance accumulates faster close to the delivery in the nonlinear (quadratic, TTM IV) cases, consistent with the market implied volatility data (see Figure 2.4) and the differences in the intermediate months are more prominent on futures with longer deliveries.

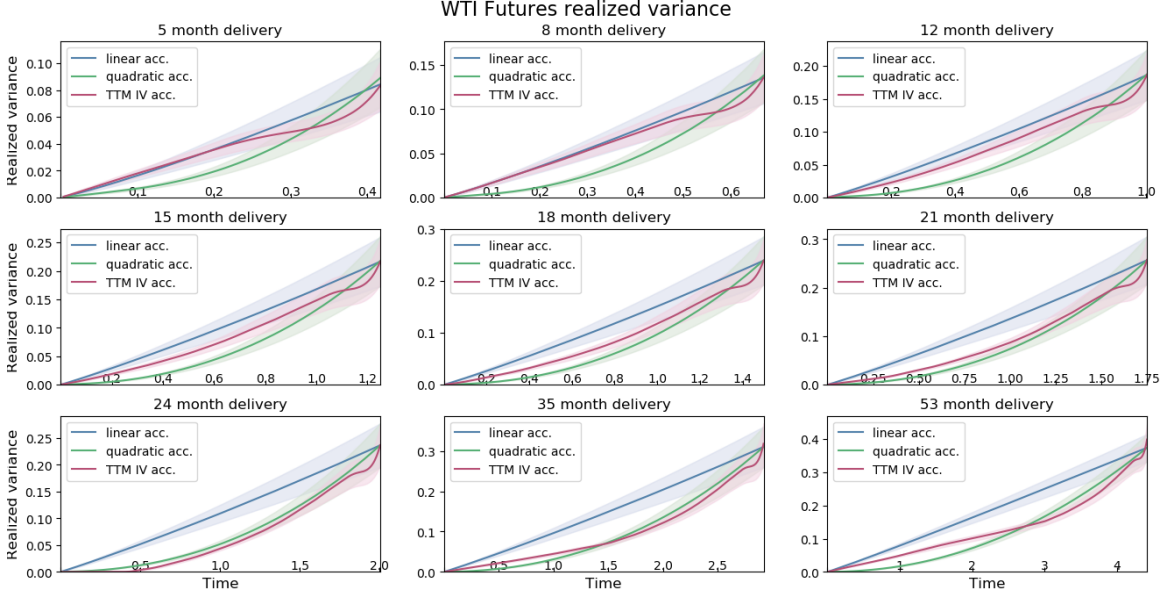


Figure 3.4: Realized variance $RV_j(t)$ for several deliveries T_j with linear, quadratic, and TTM IV accumulators. Solid lines represent the Monte Carlo mean for 10000 paths, and the shaded areas span one standard error around the mean.

For the stochastic rate case, we assume that the domestic short rate follows a G1++ process⁴

$$\begin{aligned} r(t) &= x(t) + \phi_t, \\ dx(t) &= -ax(t)dt + \sigma dW^r(t), \end{aligned} \tag{3.15}$$

where W^r is a Brownian motion under risk-neutral measure \mathbb{Q} , ϕ_t is the shift function that ensures $P(0, t) = \mathbf{E}^{\mathbb{Q}}[D(t)]$, a is the mean reversion coefficient, and σ is the volatility coefficient. In our tests, the parameters are chosen as $a = 0.02$, $\sigma = 0.01$, and the coefficients of correlation between the Brownian motions, defined as in $d\langle W^1, W^r \rangle_t = \rho_{1r}dt$, and $d\langle W^2, W^r \rangle_t = \rho_{2r}dt$, are set as $\rho_{1r} = \rho_{2r} = -0.2$. The expectation appearing in (3.12) is estimated by simulating 1000 Monte Carlo paths and their antithetic conjugates. We calibrate the WTI leverage functions with the TTM IV accumulator (3.8), whereas for calibrating the NG leverage functions we choose the quadratic accumulator (3.7).

The calibrated leverage functions are validated by simulating the model, with 10000 paths and their antithetic conjugates, to price vanilla call options at various moneynesses and maturities. For the deterministic rate case, Figure 3.5 shows that the market prices are

⁴G1++ can be seen as a reparametrization of Hull-White or LGM models. Any other calibrated interest model could also be used as long as short rate and its time integral can be simulated.

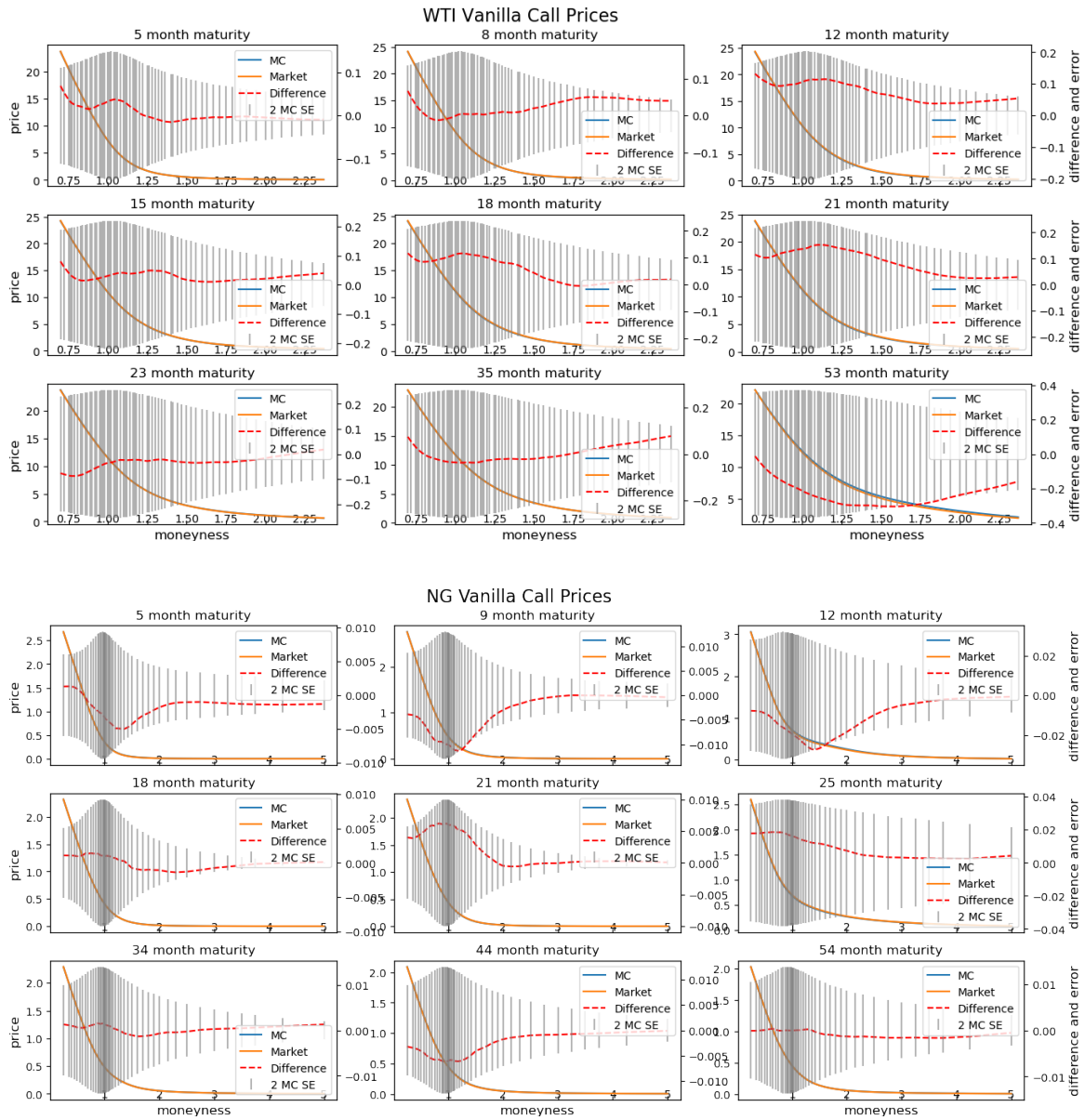


Figure 3.5: Market and Monte Carlo prices for vanilla call options on WTI and NG futures at various maturities. Rate is deterministic. We simulate 10000 paths and their antithetic conjugates to compute the Monte Carlo estimates and standard errors for prices.

within two Monte Carlo standard errors of the simulated prices for most strikes in the test range. Similarly for the stochastic rate case, as shown in Figure 3.6, the market prices are within two Monte Carlo standard errors of the simulated prices.

These results show that the calibrated leverage functions recover the market volatility smile well, and that the stochastic rate does not introduce significant inaccuracy to the model.

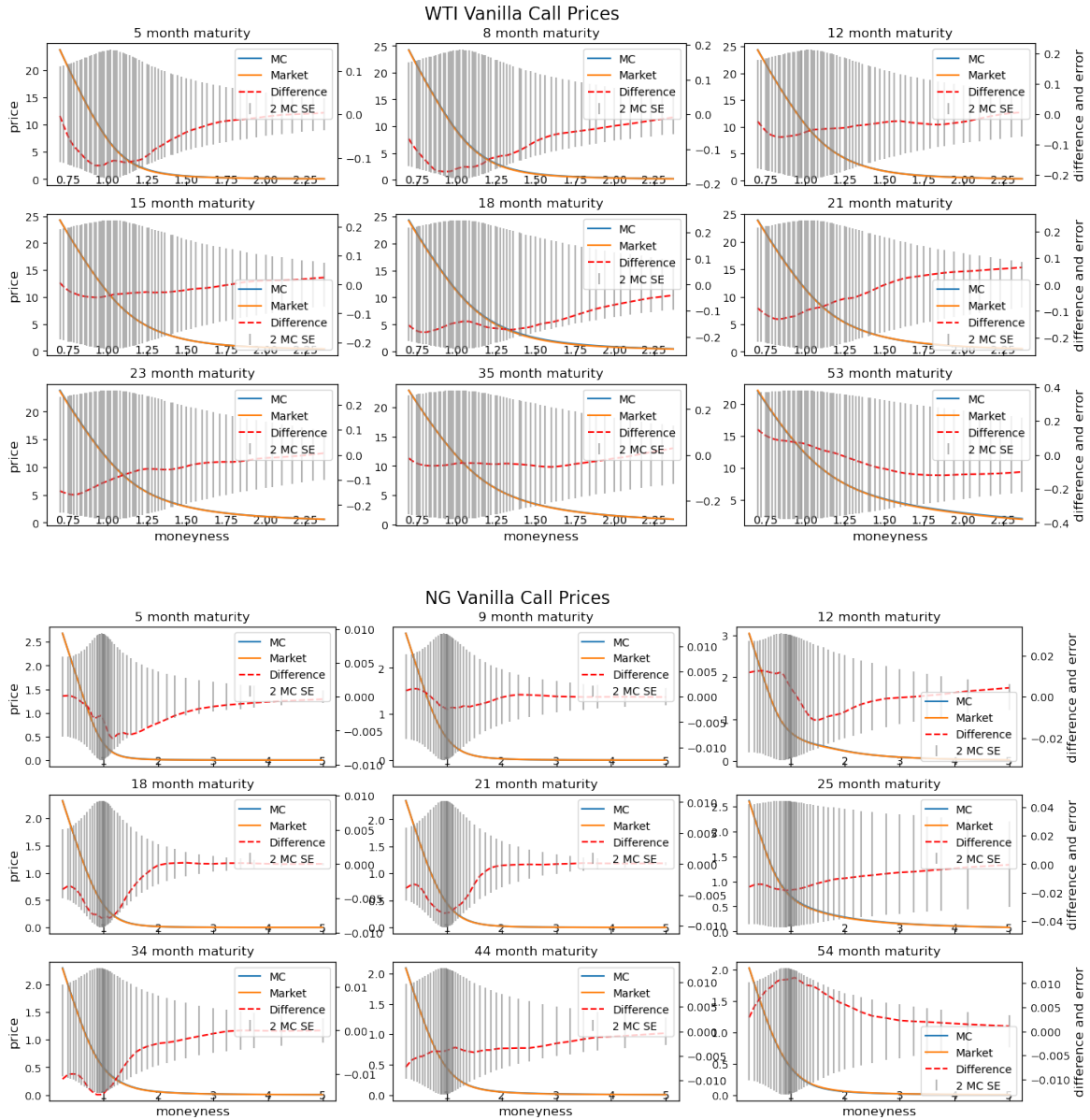


Figure 3.6: Market and Monte Carlo prices for vanilla call options on WTI and NG futures at various maturities. The stochastic short rate follows a G1++ process. We simulate 10000 paths and their antithetic conjugates to compute the Monte Carlo estimates and standard errors for prices.

4 Discussion

The demonstration of price recovery shows that the calibrated model captures WTI and NG market volatility smiles in both deterministic and stochastic rate cases. While remaining in the risk-neutral framework, the total implied variance for the entire maturity determined during the model calibration from market data can be accumulated over time in different

ways. For instance, one can use the total implied variance from other futures options with shorter time-to-maturity to define the accumulation over the longer option maturity, reflecting information from all implied volatility slices. This can result in models where the total implied volatility accumulates faster than linearly close to the corresponding futures option maturity, which is commonly referred to as the Samuelson or maturity effect. We also mentioned other ways to directly control the accumulation of total implied variance. Further studies showed that the market prices are recovered comparably well to the linear interpolation case when the total implied variance is interpolated with the suggested methodology which gives rise to higher realized volatilities towards maturity.

One can further generalize the smile dynamics by adding stochasticity to the diffusion process (3.1),

$$dF_j(t) = F_j(t)\sqrt{U_j(t)}L_j(F_j(t), t) [\sigma_1(t, T_j)dW_1(t) + \sigma_2(t, T_j)dW_2(t)], \quad (4.1)$$

where $U_j(t)$ are adapted processes that model the stochastic variance. A typical choice would be the CIR process [15] with the $U_j(t)$ process parameters calibrated to near at-the-money vanilla options with maturity T_j . For this extended model, the leverage functions are given by [11]

$$L_j(K, t)^2 = \frac{P(t, T_j) \left(\frac{\partial C_j}{\partial t} + \mathbf{E}^{\mathbb{Q}} \left[D(t)(F_j(t) - K)r(t)\mathbf{1}_{F_j(t) > K} \right] \right)}{\frac{1}{2}K^2 \frac{\partial^2 C_j}{\partial K^2} [\sigma_1(t, T_j)^2 + \sigma_2(t, T_j)^2] \mathbf{E}^{\mathbb{Q}} [D(t)U_j(t)|F_j(t) = K]}, \quad (4.2)$$

where the expectations are taken under risk-neutral measure \mathbb{Q} . The calibration of the leverage functions proceeds as before. Only this time, one additionally needs to compute the value of the conditional expectation appearing in the above expression. Since this is a multi-dimensional problem, one can employ Monte Carlo methods, such as the binning or the regression based techniques proposed in [14] to estimate the value of this conditional expectation.

Acknowledgments The authors thank Agus Sudjianto for supporting this research, and Vijayan Nair for his comments and suggestions regarding this research. Any opinions, findings and conclusions or recommendations expressed in this material are those of the authors and do not necessarily reflect the views of Wells Fargo Bank, N.A., its parent company, affiliates and subsidiaries.

References

- [1] J. Gabillon. *The term structure of oil futures prices*. OIES: M17. Oxford Institute for Energy Studies, 1991.
- [2] Leif Andersen. Markov models for commodity futures: theory and practice. *Quantitative Finance*, 10(8):831–854, 2010.
- [3] Emanuele Nastasi, Andrea Pallavicini, and Giulio Sartorelli. Smile Modeling In Commodity Markets. *International Journal of Theoretical and Applied Finance (IJTAF)*, 23(03):1–28, May 2020.

- [4] Alberto Manzano, Emanuele Nastasi, Andrea Pallavicini, and Carlos Vázquez. Pricing commodity index options, 2022. arXiv:2208.01289.
- [5] Lorenz Schneider and Bertrand Tavin. Seasonal stochastic volatility and the Samuelson effect in agricultural futures markets, 2018. arXiv:1802.01393.
- [6] Lorenz Schneider and Bertrand Tavin. Seasonal stochastic volatility and correlation together with the Samuelson effect in commodity futures markets, 2015. arXiv:1506.05911.
- [7] Lorenz Schneider and Bertrand Tavin. From the Samuelson volatility effect to a Samuelson correlation effect: Evidence from crude oil calendar spread options, 2014. arXiv:1401.7913.
- [8] Sergiy Ladokhin and Svetlana Borovkova. Three-factor commodity forward curve model and its joint P and Q dynamics. *Energy Economics*, 101:105418, 2021.
- [9] Ole E. Barndorff-Nielsen, Fred Espen Benth, and Almut E. D. Veraart. Modelling energy spot prices by volatility modulated Lévy-driven Volterra processes. *Bernoulli*, 19(3):803–845, 2013.
- [10] Lingfei Li and Vadim Linetsky. Time-changed Ornstein-Uhlenbeck processes and their applications in commodity derivative models. *Mathematical Finance*, 24(2):289–330, 2012.
- [11] Orcan Ögetbil. Extensions of Dupire Formula: Stochastic Interest Rates and Stochastic Local Volatility, 2020. arXiv:2005.05530.
- [12] Edouard Jaeck and Delphine Lautier. Samuelson hypothesis and electricity derivative markets. In *31st International French Finance Association Conference, AFFI 2014*, page 24, 2014.
- [13] Elton Daal, Joseph Farhat, and Peihwang P Wei. Reexamining the maturity effect using extensive futures data. *Department of Economics and Finance Working Papers, The University of New Orleans, 1991-2006. Paper 12.*, 2003.
- [14] Orcan Ögetbil, Narayan Ganesan, and Bernhard Hientzsch. Calibrating local volatility models with stochastic drift and diffusion. *International Journal of Theoretical and Applied Finance*, 25(02):2250011, 2022.
- [15] John C. Cox, Jonathan E. Ingersoll, and Stephen A. Ross. A Theory of the Term Structure of Interest Rates. *Econometrica*, 53(2):385–407, 1985.